Effects of Three Typical Resistivity Models on Pulsed Inductive Plasma Acceleration Modeling *

Xin-Feng Sun(孙新锋)[1], Yan-Hui Jia(贾艳辉)[1], Tian-Ping Zhang(张天平)[1], Chen-Chen Wu(吴辰宸)[1], Xiao-Dong Wen(温晓东)[1], Ning Guo(郭宁)[1], Hai Jin(金海)[2]**, Yu-Jun Ke(柯于俊)[1], Wei-Long Guo(郭伟龙)[1]

[1]*National Key Laboratory of Science and Technology on Vacuum Technology and Physics, Lanzhou Institute of Physics, Lanzhou 730000*

[2]*College of Electrical and Information Engineering, Lanzhou University of Technology, Lanzhou 730050*

(Received 13 July 2017)

The effects of three different typical resistivity models (Spitzer, Z&L and M&G) on the performance of pulsed inductive acceleration plasma are studied. Numerical results show that their influences decrease with the increase of the plasma temperature. The significant discriminations among them appear at the plasma temperature lower than 2.5 eV, and the maximum gap of the pulsed inductive plasma accelerated efficiency is approximately 2.5%. Moreover, the pulsed inductive plasma accelerated efficiency is absolutely related to the dynamic impedance parameters, such as voltage, inductance, capacitance and flow rate. However, the distribution of the efficiency as a function of plasma temperature with three resistivity models has nothing to do with the dynamic impedance parameter.

PACS: 52.75.Di, 51.50.+v, 52.25.Jm, 52.80.Yr DOI: 10.1088/0256-307X/34/12/125202

The pulsed inductive accelerated plasma has been employed to produce the thrust for spacecraft propulsion devices for more than five decades. The development of this concept was firstly directed by Dailey and Lovberg of TRW space systems in Redondo beach in 1964.[1–3] Since then, the pulsed inductive acceleration propulsion has made great progress in both experiments and theories.[4] The propulsion data representing the state-of-the art of pulsed inductive acceleration has achieved efficiency of about 50% with a broad specific impulse range of 2000–8000 s.[4–6]

In this duration, the theoretical modeling analysis has also been introduced to aid the optimal design for the progress of engineering and experiment. In the early 1980s, a one-dimensional (1D) pulsed inductive acceleration model that is based on circuit equation has been developed to learn the physics of inductive plasma at the TRW company.[3,4] The numerical results by solving the coupling momentum and circuit equations agree well with the performance test results. In the late 1990s, a two-dimensional (2D) axial symmetric time-dependent magnetohydrodynamic (MHD) fluid code multiblock arbitrary coordinate hydromagnetic (MACH2) was used to simulate the pulsed inductive acceleration plasma. It was confirmed that the experimental observation of the sum of all energy sinks was independent of operating conditions.[7,8] In 2007, the thermodynamics model of argon was added to MACH2 code, which is helpful to study the ionization and acceleration processes of physics more accurately and effectively.[8] As a result, the influence factor on the efficiency of the plasma acceleration was investigated. In 2008, the MACH2 code was utilized to predict the operation at low energy for a range of propellants and propellant mass values for pulsed inductive plasma.[9] In 2007, the general equation and mesh solver (GEMS) were used for the pulsed inductive acceleration in Purdue University.[10] The electric field, magnetic field and displacement current of the inductive acceleration coils were gained by solving the full Maxwell equation. In 2012, the PIC code was adopted to research the pre-ionization physical process for conical coils at Missouri University of Science and Technology.[11] They found that the bias field would inhibit the pre-ionization process of plasma if the electric field is mismatched.

Polzin *et al.* optimized the 1D TRW acceleration model by adding the plasma equations and the external magnetic field equation.[4,12–14] However, it cannot be applied to simulate the production, formation and acceleration of conical pinch plasma current sheet due to its radial direction movement and force. Therefore, Hallock and Polzin upgraded the 1D model to a 2D one.[4,15,16] To understand the mechanism of energy exchange and transport of pulsed inductive plasma current sheet as time evolution, Polzin *et al.* have studied the effects of two different resistances modeled on the energy sink and calculation accuracy by adding the energy equation to the previous 1D model. However, the influences of different resistive models on pulsed inductive plasma acceleration performance have never been surveyed. The purpose of this work is to study the effects of three typical resistivity models on 1D pulsed inductive plasma acceleration.

In this Letter, a 1D acceleration model is introduced. Then, three resistivity models and some discussions are given. Finally, the calculation results are discussed.

An equivalent lumped element circuit model of a pulsed inductive accelerator is given in Fig. 1. By applying Kirchoff's law to each loop in Fig. 1, the follow-

*Supported by the Fund of Science and Technology on Vacuum Technology and Physics Laboratory of Lanzhou Institute of Physics under Grant No YSC0715, the National Natural Science Foundation of China under Grant No 62601210, and the Civil Aerospace Technology Research Project under Grant No D010509.

**Corresponding author. Email: jinhai@hust.edu.cn

ing coupled first-order ordinary differential equation can be obtained,[4,13]

$$\begin{aligned}\frac{dI_1}{dt} &= [VL_c + (MI_1 + I_2L_c)(dM/dt) - I_2MR_p \\ &\quad - I_1R_eL_c]/[L_c(L_0 + L_c) - M^2], \\ \frac{dI_2}{dt} &= \frac{M(dI_1/dt) + I_1(dM/dt) - I_2R_p}{L_c}, \\ \frac{dV}{dt} &= \frac{-I_1}{C}, \end{aligned} \tag{1}$$

where V is the voltage on the capacitor, C is the capacitance, L_0 is the external inductance, L_c is the acceleration coil inductance, the plasma inductance is also equal to L_c, I_1 is the current of external circuit, I_2 is the current of plasma current sheet, R_e and R_p are the external and plasma resistance, respectively.

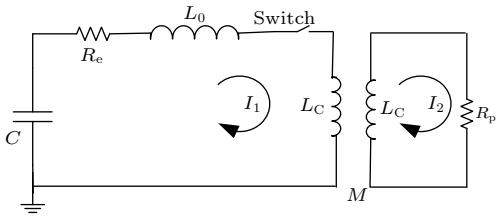

Fig. 1. Equivalent lump electrical circuit model of a pulsed inductive accelerator.[4,12–14]

A simple experimental model has been used since the inductance between coil and the plasma current sheet is difficult to solve with an analytic solution. The changing mutual inductance equation can be solved as[4,12–16]

$$\frac{dM}{dt} = -\frac{L_C}{2z_0}\exp\Big(-\frac{z}{2z_0}\Big)\frac{dz}{dt}, \tag{2}$$

where z is the axial current sheet position, z_0 is the decoupled length, and the experimental model is defined as

$$L_{\text{total}} = L_0 + L_C(1 - \exp(-z/z_0)). \tag{3}$$

It is assumed that all of the neutral propellant that the current sheet encounters can be entrained and accelerated, while only a fraction of the gas can be accelerated in a real situation. The changing mass of the current sheet with time is written as[13]

$$\frac{dm}{dt} = \rho_A f(z) v_z, \tag{4}$$

where v_z is the sheet velocity. If $\delta_m \geq z$, then $\rho_A f(z) = \rho_0(1 - z/\delta_m)$, and δ_m/z_0 will be equal to 0.53. Otherwise, $\rho_A f(z) = 0$.

The momentum equations are written as

$$\begin{aligned}\frac{dv_z}{dt} &= \Big[\frac{L_cI_1^2}{2z_0}\exp\Big(-\frac{z}{z_0}\Big) \\ &\quad - \rho_A v_z^2 - p_A\pi(b^2 - a^2)\Big]/m, \end{aligned} \tag{5}$$

$$\frac{dz}{dt} = v_z. \tag{6}$$

The first term on the right of Eq. (5) represents the electromagnetic force, the second term represents the neutral entrainment gas momentum, and the last term represents the pressure. Here P_A can be solved from the ideal gas equation of state,[16]

$$P_A = \frac{\rho_A}{\pi(b^2 - a^2)}\frac{k_B}{M_c}T_A, \tag{7}$$

where k_B is the Boltzmann constant,[17,18] T_A is the temperature of neutral gas, b and a are the outer and inner coil radii, and M_c is the atomic or molecular mass.

The plasma resistance is defined as

$$R_p = \frac{\pi\eta(b + a)}{\delta_a(b - a)}, \tag{8}$$

where η is the resistivity, δ_a is the thickness of current sheet,[16]

$$\delta_a(t) = \sqrt{\eta(t + t_0)/\mu_0},\ t_0 = \mu_0\delta_s^2/\eta, \tag{9}$$

with δ_s being the initial value of δ_a at time $t = 0$.

To identify the influences of some relevant scaling parameters on the pulsed inductive plasma acceleration performance, all of the governing equations are normalized as the following dimensionless variables: $I_1^* = (L_0/C)^{0.5}I_1/V_0$, $I_2^* = (L_0/C)^{0.5}I_2/V_0$, $t^* = t/(L_0/C)^{0.5}$, $z^* = z/z_0$, $V^* = V/V_0$, $M^* = M/L_C$, $L^* = L_0/L_C$, $m^* = m(t)/m_{\text{bit}}$, $m_0^* = m_0/m_{\text{bit}}$, $\rho^* = \rho z_0/m_{\text{bit}}$, $v_z^* = v_z(L_0C)^{0.5}/z_0$, $\psi_1 = R_e(C/L_0)^{0.5}$, $\psi_2 = (C/L_0)^{0.5}$, $\alpha = (CV_0)^2L_C/(2m_{\text{bit}}z_0^2)$, $\beta = (k_BT_ACL_0)/(M_cz_0^2)$.

By substituting these dimensionless variables into Eqs. (1)–(7) and applying some algebraic operations, we obtain the nondimensional differential equations as

$$\begin{aligned}\frac{dI_1^*}{dt^*} &= [V^*L^* + (M^*I_1^* + I_2^*)(dM^*/dt^*) \\ &\quad - L^*(I_2^*M^*\psi_2R_p + I_1^*\psi_1)] \\ &\quad /[(L^* + 1) - (M^*)^2], \end{aligned} \tag{10}$$

$$\frac{dI_2^*}{dt^*} = M^*\frac{dI_1^*}{dt^*} + I_1^*\frac{dM^*}{dt^*} - I_2^*L^*\psi_2R_p, \tag{11}$$

$$\frac{dV^*}{dt^*} = -I_1^*, \tag{12}$$

$$\frac{dM^*}{dt^*} = -\frac{1}{2}\exp\Big(-\frac{z^*}{2}\Big)v_z^*, \tag{13}$$

$$\begin{aligned}\frac{dv_z^*}{dt^*} &= [\alpha(I_1^*)^2\exp(-z^*) - \rho^*f(z^*)(v_z^*)^2 \\ &\quad - \rho^*f(z^*)\beta]/m^*, \end{aligned} \tag{14}$$

$$\frac{dz^*}{dt^*} = v_z^*, \tag{15}$$

$$\frac{dm^*}{dt^*} = \rho^*f(z^*)v_z^*. \tag{16}$$

The complete governing equations are set in Eqs. (10)–(16), and the effect of temperature and resistivity on exhaust velocity and the efficiency can be identified by solving the governing equations with the numerical method.

The Spitzer resistivity for the fully ionized gases is widely recognized and is sufficiently simple to estimate the resistance of the ideal plasma. However, it is not valid for the non-ideal (high plasma density and low plasma temperature (1–5 eV)) plasma with the noticeable differences from experimental results. The non-ideal plasma is characterized by a nondimensional parameter γ ($\gamma = e^2(n_\mathrm{i}+n_\mathrm{e})^{1/3}/4\pi\varepsilon_0 k_\mathrm{B}T$, where ε_0 is the vacuum dielectric constant, T is the plasma temperature (K), n_e and n_i are the plasma electron and ion density (m^{-3}), respectively): ideal $\gamma < 0.1$; weakly non-ideal $0.1 < \gamma < 1$; strongly non-ideal $\gamma > 1$.[19] Thus many researchers have devoted to correcting the Spitzer modeling by calculating the conductivities of non-ideal plasmas since it is of importance in plasma discharges. In this work, three mainly different resistivity models are chosen for study, and the three resistivity models will be introduced in detail in the following.

Spitzer modeling reads[20]

$$\eta = 38Z\ln\Lambda/(\gamma_\varepsilon T^{3/2}),\ (\Omega\cdot\mathrm{m}), \tag{17}$$

where γ_ε is a correct factor that takes into the electron–electron collision, $\ln\Lambda = \ln(1.24\times 10^7 T^{3/2}/n_\mathrm{e}^{1/2})$ is the Coulombic logarithmic term, and Z is the mean ionic charge.

It is not difficult to find that the conductivity $\sigma = 1/\eta$ will become infinite and the resistivity will vanish as $\Lambda \to 1$ in the non-ideal plasma region from Eq. (17). Obviously, this result is nonsense. Hence, it is the major difficulty for the Spitzer resistivity modeling.

Z&L modeling reads[21]

$$\eta = 38.0Z\ln(1+1.4\Lambda_\mathrm{m}^2)^{1/2}/(\gamma_\varepsilon T^{3/2}\ (\Omega\cdot\mathrm{m}), \tag{18}$$

where $\Lambda_\mathrm{m} = (\lambda_2^+ + \lambda_\mathrm{D}^2)^{0.5}/b_0$ is the correction of the Coulombic logarithmic term, $b_0 = Ze^2/(12\pi\varepsilon_0 k_\mathrm{B}T)$ is the collision parameter, $\lambda_\mathrm{D} = [(\varepsilon_0 k_\mathrm{B}T)/(n_\mathrm{e}e^2)]^{0.5}$ is the plasma Debye length, e is the electron charge, $\lambda_+ = (4\pi n_+/3)^{-1/3}$ is the mean ionic radius of the charged ion density, and n_+ is the ion density.

Zollweg and Liebermann modify the Spitzer resistivity model by re-evaluating the Coulomb logarithm term and using a heuristic screening radius model. It extends the Spitzer model to the non-ideal region, and the formation of Eq. (18) is also further simplified.

M&G modeling reads[19]

$$\eta = 1/\Big[\sigma_0\delta\exp(\Delta\mu/k_\mathrm{B}T)\Big(1-\frac{(\omega/k_\mathrm{B}T)^4}{(\omega/k_\mathrm{B}T+0.8)^4}\Big)\Big], \tag{19}$$

where $\Delta\mu = (r_\mathrm{s}k_\mathrm{B}T)/(\lambda_\mathrm{D}N_\mathrm{D}/3)$ is the chemical potential due to the interactions, N_D is the number of charged particles in a Debye sphere, $\omega = [r_\mathrm{s}(k_\mathrm{B}T)^2/(3\lambda_\mathrm{D}N_\mathrm{D})]^{0.5}$ is the energy dispersion from plasma oscillations, $r_\mathrm{s} = \lambda_\mathrm{D}[1+\pi^2Z^{3/2}\gamma^{3/2}/(2+2Z)^{0.5}/8]\ln[1+(r_\mathrm{s}/\lambda_\mathrm{D})^2\gamma^3]$ is the non-Debye screening radius, $\delta = \ln\Lambda/\ln[1+1.4(r_\mathrm{s}/\lambda_\mathrm{D})^2\Lambda^2]^{0.5}$, and $\Lambda = \lambda_\mathrm{D}/b_0$.

It is significant that the resistivity is directly related to the plasma temperature of the above three modeling equations. Thus it is necessary to investigate the effect of the plasma temperature on the different resistivity models. We set the plasma temperature to 1–5 eV according to many of the experimental results. The resistivity equations are solved as a function of the temperature by MATLAB and the computed results are displayed in Fig. 2.

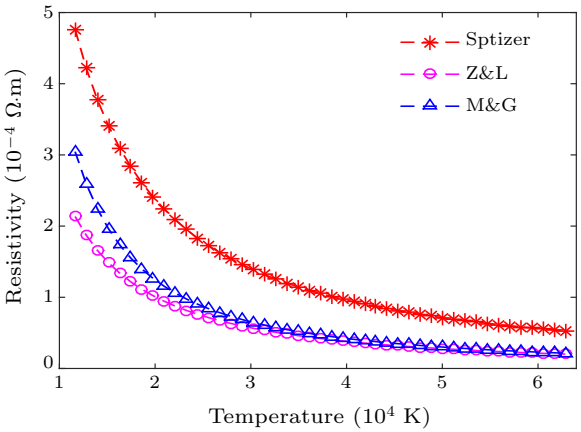

Fig. 2. Comparison of three resistivity models as a function of plasma temperature.

It should be pointed out that all of the parameters in our calculations are in MKS units. The mean ionic charge Z is set to 1, γ_ε is equal to 0.9, and the plasma density is $1\times 10^{21}\,\mathrm{m}^{-3}$. In Fig. 2, the red dashed line with stars represents the Spitzer resistivity, the pink dashed line with circles stands for the Z&L modeling, and the blue dashed line with triangles is the M&G modeling. From the comparison of these resistivity models, it is easy to find that the resistivity decreases with the increase of the temperature. However, the Spitzer resistivity is distinctly different from the other two models due to its larger values. At the regions of plasma temperature larger than 3×10^4 K, the Z&L and M&G models are completely consistent, while in the low temperature regions of $T < 3\times 10^4$ K, the distinction of the three resistivity is striking. Therefore, it will be worth studying the effect of the resistivity on the performance of the pulsed inductive plasma acceleration if the plasma temperature is between 1 and 2.5 eV ($\approx 3\times 10^4$ K).

The complete dimensionless differential equations and resistivity model for pulsed inductive plasma have been given above. Thus the first and most important thing is to solve these equations by a set of proper initial conditions and to validate their rationality. Unluckily, it is difficult to solve the equations with an analytic method. However, the MATLAB ODE five-order Runge–Kutta method provides us with an opportunity to calculate these equations with a shortcutting way. The results of non-dimensional parameters as a function of time are plotted in Fig. 3. Three different values of $\psi_1 = \psi_2$ are given as 0.1, 0.25 and 0.5. The curves are circuit current I_1^*, plasma current I_2^*, capacitor voltage V^*, current sheet position z^*, current sheet velocity v_z^*, and mutual inductance M^* in Fig. 3.

It is obvious that the currents (I_1^* and I_2^*) increase

with the decrease of the values of ψ_1 and ψ_2 in Fig. 3. This means that more of the external circuit energy will transfer to the current sheet kinetic energy as the decrease of ψ_1 and ψ_2. This is the reason why the velocity is the largest when $\psi_1 = \psi_2 = 0.1$. Moreover, the velocity will stop rising with the reversal of the capacitor voltage after the first half-cycle at the time of $t^* = 4$, even if the external circuit current is maintained. Therefore, the higher peak current and lower current pulse will benefit the pulsed inductive plasma acceleration efficiency. All of these results are in accordance with Polzin's work,[4,13] which demonstrates the correction of our numerical results and model equations.

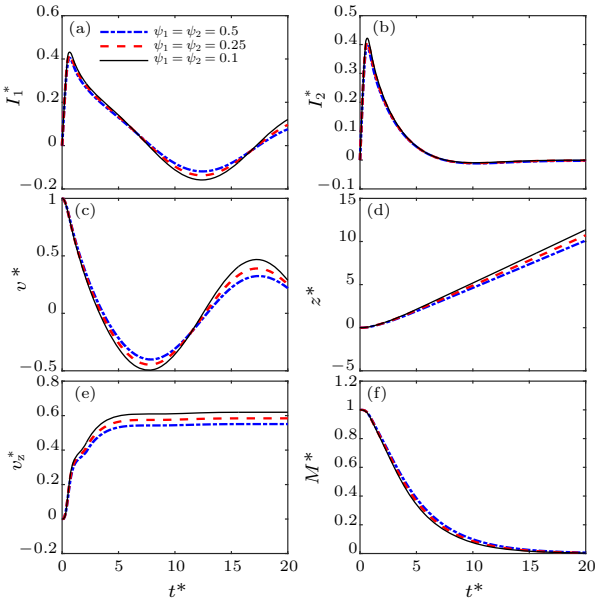

Fig. 3. Non-dimensional parameters as a function of time in a pulsed inductive accelerated plasma for different values of ψ_1 and ψ_2. The values of α, β and L^* are of 2.1, 0.0025 and 0.121, respectively.

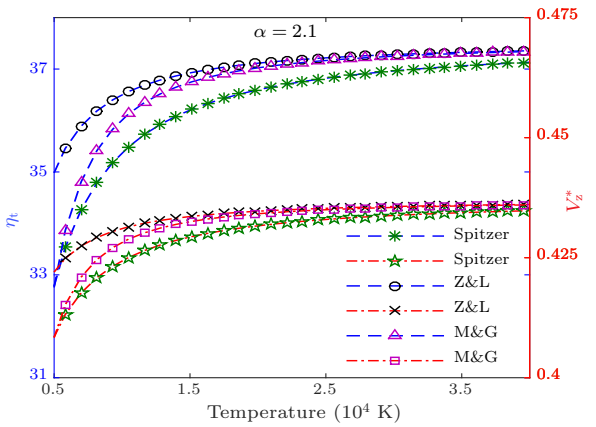

Fig. 4. Non-dimensional parameter V_z^* and the efficiency η_t as a function of plasma temperature in a pulsed inductive accelerated plasma for different resistivity modelings. The values of ψ_1, ψ_2, α, β, L^*, R_1 and R_2 are 0.2, 0.2, 2.1, 0.0025, 0.121, 0.2 and 0.5, respectively.

On the basis of the previous studies, the effect of plasma temperature on inductive acceleration efficiency ($\eta_t = m^* v_z^{*2}/(2L^*\alpha)$) and exhaust velocity will be further studied. The efficiency and exhaust velocity are the two most important parameters for the inductive plasma acceleration thruster. The values of ψ_1, ψ_2, α, β, L^*, R_1 and R_2 are 0.2, 0.2, 2.1, 0.0025, 0.121, 0.2 and 0.5, respectively. The plasma temperature is set to 0.5–3.7 eV, which includes the above temperature of 1–2.5 eV. The left vertical axis is the percentage efficiency and the right vertical axis means the non-dimensional exhaust velocity in Fig. 4. The top three blue dashed curves are the variations of inductive acceleration efficiency with the plasma temperature for different resistivity models. The circles, triangles, and stars indicate the Z&L, M&G, and Spitzer models, respectively.

In Fig. 4, we observe that the maximum gap of the efficiency between the Z&L and Spitzer models is about 2.5% at 0.5 eV, and the influences of the three different models on inductive acceleration efficiency become weaker with the increase of the temperature. The simple reason can be comprehended from Eqs. (17)–(19) that the resistivity decays exponentially with the increase of the plasma temperature. Similarly, the role of different resistivity models on pulsed inductive acceleration efficiency is not obvious when the temperature is greater than 2.5 eV, and the efficiency with the Spitzer resistivity model is the least.

The three red dashed curves on the bottom of Fig. 4 are the variations of non-dimensional exhaust velocity with the plasma temperature for different resistivity models. The crosses, rectangles, and stars indicate the Z&L model, M&G model, and Spitzer model, respectively. The discrimination of the models on the non-dimensional exhaust velocity is similar to the efficiency. The greatest velocity distance is 0.0175 between Z&L and Spitzer models. Therefore, it will be meaningless to focus on the influence of resistance if the temperature is higher than 2.5 eV according to these two calculation results.

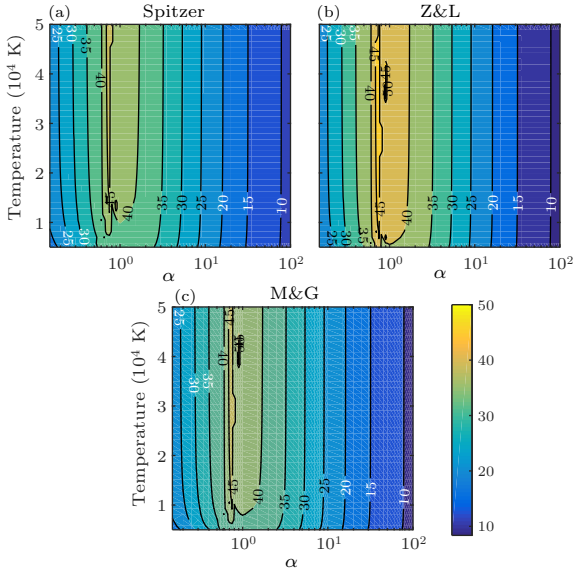

Fig. 5. Contours of the inductive acceleration efficiency for varying of plasma temperature and dynamic impedance parameter α.

The computed inductive acceleration efficiencies

of three different resistivity models are contoured by varying of plasma temperature and dynamic impedance parameter α which has been confirmed to be an important variable in Fig. 5.[4] The values of the efficiency are marked on the equipotential lines. It is shown that the inductive acceleration efficiency has a local maximum value with the variation of α. In our computations, the optimal value of α is about 1.0 from the numerical results with diverse models. Moreover, it is clear that the influence of the temperature is noticeable among these three models. However, the effect of temperature on the efficiency is negligible beyond the region of α of approximately 1.0. The interpretation is that the plasma temperature is placed at a constant in our simulations, and the energy conversion is ignored with the lack of the energy equation. This deficiency will be resolved by the optimization of the modeling equations.

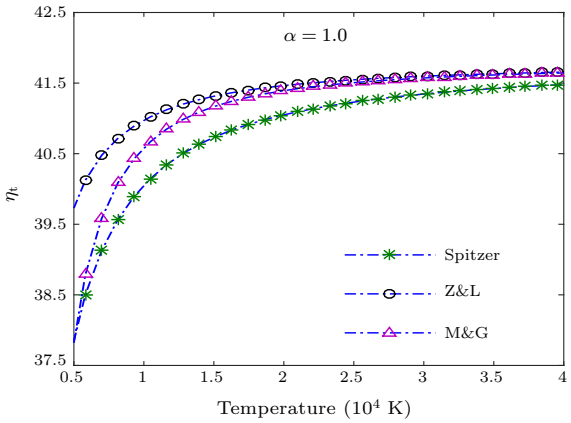

Fig. 6. The efficiency η_t as a function of plasma temperature in a pulsed inductive accelerated plasma for different resistivity models. The values of ψ_1, ψ_2, α, β, L^*, R_1 and R_2 are 0.2, 0.2, 1.0, 0.0025, 0.121, 0.2 and 0.5, respectively.

The calculation results have shown that the optimal value of α is about 1.0 in Fig. 5. Therefore, it is necessary to investigate the effect of the plasma temperature on the inductive accelerated efficiency of three different resistivity models. The computed results are posted on Fig. 6. Compared with the results in Fig. 4, it is easy to find that the maximum efficiency rises up to 41.5% in Fig. 6, i.e., it has been enlarged about 5%. However, the inductive accelerated efficiency is not the optimum value at the presentation of Fig. 6, because the best performance of the efficiency is greater than 45% corresponding to the computation results in Fig. 5. This result further illustrates that the efficiency is susceptible to dynamic impedance parameter α.

It should be noted that the tendencies of the curves for three resistivity models in Fig. 6 are the same as those in Fig. 4, which reveal that the distribution of efficiency along with plasma temperature will not be affected by the dynamic impedance parameter. Meanwhile, the optimal value of α is not a constant for all the situations and is related to many other parameters, such as ψ_1, ψ_2, L^*, $m_{\rm bit}$ and z_0. It can be optimized by the limitation of the expression of $\alpha = (CV_0)^2 L_{\rm C}/(2m_{\rm bit} z_0^2)$.

In summary, the effects of three typical resistivity models (Spitzer, Z&L, and M&G) on pulsed inductive plasma accelerated modeling have been studied in this work. The results show the effect of different resistivity models on the performance of the pulsed inductive plasma accelerated efficiency is significant as the plasma temperature is between 1 and 2.5 eV, and the influences of the resistivity on inductive acceleration efficiency will become weaker with the increase of the temperature. Thus it is meaningless to focus on the influence of resistance if the temperature is higher than 2.5 eV. Moreover, the numerical results also indicate that the inductive accelerated efficiency with the simple Spitzer model is inappropriate, and the maximum differences of the pulsed inductive plasma accelerated efficiency among these three models are about 2.5%. In addition, the inductive plasma accelerated efficiency is associated distinctly with the dynamic impedance parameter. However, the dynamic impedance parameter will not affect the distribution of the efficiency, which only varies as a function of plasma temperature.

References

[1] Dailey C L and Lovberg R H 1972 *AIAA J.* **10** 125
[2] Dailey C L and Davis H A 1982 *16th Int. Electric Propulsion Conf.* (New Orleans Am. 17–19 November 1982) p 192
[3] Lovberg R H and Dailey C 1982 *AIAA J.* **20** 971
[4] Polzin K A 2011 *J. Propulsion Power* **27** 513
[5] Dailey C L and Lovberg R H 1993 *NASA Contractor Report* (NASA USA 1993) p 191155
[6] Lovberg R H and Dailey C L 2000 *NASA Contractot Report* (NASA USA 2000) p 210573
[7] Peterkin R E, Frese M H and Sovinec C R 1998 *J. Comput. Phys.* **140** 148
[8] Mikellides P G and Ratnayake N 2007 *J. Propulsion Power* **23** 854
[9] Villarreal J K 2009 *47th AIAA Aerosp. Sci. Meeting Including New Horizons Forum Aerosapce Exposition* (Orlando, USA 5–8 January 2009) p 201
[10] Corpening J, Li D, Hrbud I and Merkle C 2007 *43rd AIAA/ASME/SAE/ASEE Joint Propulsion Conf. Exhibit* (Cincinnati, USA 8–11 July 2007) p 5286
[11] Meeks W C and Rovey J L 2012 *50th AIAA Aerosp. Sci. Meeting Including New Horizons Forum Aerosp. Exposition* (Nashville, USA 9–12 January 2012) p 0514
[12] Polzin K A and Choueiri E Y 2006 *IEEE Trans. Plasma Sci.* **34** 945
[13] Polzin K Z 2006 *PhD Dissertation* (Princeton: Princeton University)
[14] Polzin K A 2008 *IEEE Trans. Plasma Sci.* **36** 2189
[15] Hallock A K and Choueiri E Y 2009 *45th AIAA/ASME/SAE/ASEE Joint Propulsion Conference & Exhibit* (Denver, USA 2–5 August 2009) p 5448
[16] Hallock A K and Polzin K A 2011 *8th MSS/6thLPS/5th SPS Meeting* (Huntsville, USA 5–9 December 2011) p 2197
[17] Khoramabadi M and Masoudi S F 2013 *Chin. Phys. Lett.* **30** 085202
[18] Sun S R and Wang H X 2014 *Chin. Phys. Lett.* **31** 095205
[19] Mohanti R B and Gilligan J G 1990 *J. Appl. Phys.* **68** 5044
[20] Spitzer L 1956 *Physics of Full Ionized Cases* (New York: Inter Science) chap 5 p 136
[21] Zollweg R J and Liebermann R W 1987 *J. Appl. Phys.* **62** 3621